Original Article

MOLECULAR METABOLISM

The role of C16:0 ceramide in the development of obesity and type 2 diabetes: CerS6 inhibition as a novel therapeutic approach

Suryaprakash Raichur [5,*,7], Bodo Brunner [1,7], Maximilian Bielohuby [1], Gitte Hansen [2], Anja Pfenninger [1], Bing Wang [4], Jens C. Bruning [3], Philip Just Larsen [6], Norbert Tennagels [1,]**

ABSTRACT

Objective: Ectopic fat deposition is associated with increased tissue production of ceramides. Recent genetic mouse studies suggest that specific sphingolipid C16:0 ceramide produced by ceramide synthase 6 (CerS6) plays an important role in the development of insulin resistance. However, the therapeutic potential of CerS6 inhibition not been demonstrated. Therefore, we pharmacologically investigated the selective ablation of CerS6 using antisense oligonucleotides (ASO) in obese insulin resistance animal models.

Methods: We utilized ASO as therapeutic modality, CerS6 ASO molecules designed and synthesized were initially screened for in-vitro knock-down (KD) potency and cytotoxicity. ASOs with >85% inhibition of CerS6 mRNA were selected for further investigations. Most promising ASOs verified for in-vivo KD efficacy in healthy mice. CerS6 ASO (AAGATGAGCCGCACC) was found most active with hepatic reduction of CerS6 mRNA expression. Prior to longitudinal metabolic studies, we performed a dose titration target engagement analysis with CerS6 ASO in healthy mice to select the optimal dose. Next, we utilized leptin deficiency ob/ob and high fat diet (HFD) induced obese mouse models for pharmacological efficacy study.

Results: CerS6 expression were significantly elevated in the liver and brown adipose, this was correlated with significantly elevated C16:0 ceramide concentrations in plasma and liver. Treatment with CerS6 ASO selectively reduced CerS6 expression by ~90% predominantly in the liver and this CerS6 KD resulted in a significant reduction of C16:0 ceramide by about 50% in both liver and plasma. CerS6 KD resulted in lower body weight gain and accompanied by a significant reduction in whole body fat and fed/fasted blood glucose levels (1% reduction in HbA1c). Moreover, ASO-mediated CerS6 KD significantly improved oral glucose tolerance (during oGTT) and mice displayed improved insulin sensitivity. Thus, CerS6 appear to play an important role in the development of obesity and insulin resistance.

Conclusions: Our investigations identified specific and selective therapeutic valid ASO for CerS6 ablation in in-vivo. CerS6 should specifically be targeted for the reduction of C16:0 ceramides, that results in amelioration of insulin resistance, hyperglycemia and obesity. CerS6 mediated C16:0 ceramide reduction could be a potentially attractive target for the treatment of insulin resistance, obesity and type 2 diabetes.

© 2019 The Authors. Published by Elsevier GmbH. This is an open access article under the CC BY-NC-ND license (http://creativecommons.org/licenses/by-nc-nd/4.0/).

Keywords Obesity; Insulin resistance; Type 2 diabetes; Ceramides; Sphingolipids; Antisense oligonucleotide

1. INTRODUCTION

The increasing global burden of type 2 diabetes is alarming, driving the development of novel therapeutic agents that address the inadequate efficacy and adverse effects of currently marketed insulin sensitizing agents [1]. Western-style diets, being rich in saturated fatty acids and carbohydrates, and channelizing into non-adipose tissues such as liver and skeletal muscle for storage that cause metabolic dysregulation [2–4]. Moreover, saturated fats are known to induce the sphingolipid biosynthetic pathway [5,6]. Many reports have demonstrated that oversupply of saturated fats induces excess ceramide accumulation, that leads to impaired insulin signaling and energy homeostasis, and eventually to insulin resistance and type 2 diabetes [7,8]. In this context several non-clinical pharmacological studies inhibiting ceramide biosynthesis by genetic and pharmacological approaches ameliorate atherosclerosis, hepatic steatosis, insulin resistance and obesity [9]. The primary mechanism through which ceramide promotes insulin resistance is by decreasing the activity of Akt/PKB, which is an

[1]Sanofi-Aventis Deutschland GmbH, TA Diabetes, Industriepark Höchst, D-65926 Frankfurt am Main, Germany [2]Gubra ApS, Hørsholm Kongevej 11B, 2970 Hørsholm, Denmark [3]Max Planck Institute for Metabolic Research, Gleueler Str. 50, D-50931 Cologne, Germany [4]Analytical Research & Development US Predevelopment Sciences, Sanofi, 153 Second Avenue, Waltham, MA 02451, USA [5]Evotec International GmbH, Marie-Curie-Strasse 7, 37079 Goettingen, Germany [6]Grunenthal GmbH, 52072 Aachen, Germany

[7] Authors contributed equally to this study.

*Lead Corresponding author. E-mail: Surya.Prakash@evotec.com (S. Raichur).

**Corresponding author E-mail: Norbert.Tennagels@sanofi.com (N. Tennagels).

Received August 10, 2018 • Revision received December 20, 2018 • Accepted December 21, 2018 • Available online 2 January 2019

https://doi.org/10.1016/j.molmet.2018.12.008

 © 2019 The Authors. Published by Elsevier GmbH. This is an open access article under the CC BY-NC-ND license (http://creativecommons.org/licenses/by-nc-nd/4.0/).

essential facilitator for cellular glucose uptake. Ceramide blocks the activity of Akt/PKB by independent mechanisms, i.e., by stimulation of Akt dephosphorylation via protein phosphatase 2A (PP2A) and by blocking the translocation of Akt via PKCz [10]. Additionally, a recent study suggests that double-stranded RNA-dependent protein kinase (PKR) is involved in the long-term effects of ceramides on insulin receptor substrate 1 (IRS1) [11]. Two primary pathways through which ceramides are produced in the cell are the condensation of palmitate and serine (de novo synthesis) and re-acylation of sphingosine (salvage pathway). In both cases, ceramide (dihydroceramide, in the case of the de novo synthesis pathway) is produced by ceramide synthase (CerS) through N-acylation of a sphingoid base. Mammalian CerS exists in 6 isoforms (CerS1-6) with differing binding preference for specific fatty acid chain lengths.

Ceramides and their sphingolipid products are involved in multiple fundamental cellular processes; and the estimated bioactive sphingolipid mediators range from 4,000 to 60,000 [12]. Therefore, concerns exist about potential risks or adverse effects resulting from overall inhibition of sphingolipid synthesis for the treatment of chronic diseases. Accordingly, specific inhibition of only detrimental ceramide species may represent a new strategy for therapeutic intervention. In this context, two recent studies independently confirmed that a specific ceramide species, namely C16:0 ceramide, plays a key role in the development of insulin resistance [13,14]. C16:0 ceramide contains a sphingosine backbone coupled to C16 acyl-chain synthesized by ceramide synthase 6 (CerS6). Its expression and C16:0 ceramide generation is dependent on specific physiological and pathophysiological conditions in a tissue specific manner [15]. In-vivo genetic ablation of CerS6 ameliorates insulin resistance, increases whole body energy expenditure and improves glucose homeostasis by improving the β-oxidation capacity in the liver and brown adipose tissue [14].

In the current study, we investigated if the specific inhibition of CerS6 might be suitable for a drug intervention approach using CerS6 antisense oligonucleotides (ASO) to knockdown CerS6. Plasma and liver C16:0 ceramide concentrations from ob/ob, db/db and HFD (diet induced obesity) mice and respective lean controls were analyzed by LC-MS/MS. In ob/ob and HFD obese mice, both models displaying severe insulin resistance, C16:0 ceramide concentrations were significantly higher when compared to the respective lean control mice. Therefore, we considered the ob/ob and HFD mouse models as highly suitable for the investigation of CerS6 inhibition by ASO-mediated gene knockdown. After confirmation of the successful CerS6 knockdown by ASO treatment, we subsequently investigated how this affects body weight, body composition and glucose metabolism.

2. MATERIALS AND METHODS

2.1. In-vitro experiments

For ceramide measurements following treatment with palmitic acid, 50,000 HepG2 cells/well were seeded into collagen coated 96-well plates (Greiner Bio-One #655950) in complete MEM medium (Life Technologies #41090) supplemented with 1% NEAA (Life Technologies #11140), 1% PS (Life Technologies #15140) and 10% FBS (Pan Biotech #P30-3305) and cultured for 24 h at 37 °C with 5% CO_2. Treatment with 100 μM palmitic acid (Sigma #P0500) was done in reduced MEM medium (Life Technologies #41090) supplemented with 2% NCS (Biochrom #S0123) for 0, 6, 18, 28 or 48 h at 37 °C. After washing twice with 200 μl PBS, plates were stored at −80 °C until ceramide measurement using the RapidFire system as described below.

For specificity testing of human CerS6 tool siRNAs (Ambion Silencer Select s48447, s48448 and Qiagen SI00468342) HepG2 cells were reverse transfected in 96-well plates using 0.2 μl Lipofectamine RNAiMAX and 0.1, 1 and 10 nM siRNA and incubated for 72 h at 37 °C. RNA extraction was done using the SV96 Total RNA Isolation System (Promega #Z3505) according to the manufacturer's protocol including a DNase step during the procedure. For cDNA synthesis the Reverse Transcriptase kit (#N8080234) was used from ThermoFisher. cDNA synthesis from 30 ng RNA was performed using 1.2 μl 10xRT buffer, 2.64 μl MgCl2 (25 mM), 2.4 μl dNTPs (10 mM), 0.6 μl random hexamers (50 μM), 0.6 μl Oligo(dT)16 (50 μM), 0.24 μl RNase inhibitor (20U/μl) and 0.3 μl Multiscribe (50U/μl) in a total volume of 12 μl. Samples were incubated at 25 °C for 10 min and 42 °C for 60 min. The reaction was stopped by heating to 95 °C for 5 min, mRNA levels of human CerS2, CerS5 and CerS6 were quantified by qPCR using the TaqMan Universal PCR Master Mix (#4305719) and the TaqMan Gene Expression assays Hs00371958_g1, Hs00332291_m1 and Hs00826756_m1, respectively from ThermoFisher. PCR was performed in technical duplicates with the ABI Prism 7900 under the following PCR conditions: 2 min at 50 °C, 10 min at 95 °C, 40 cycles with 95 °C for 15 s and 1 min at 60 °C. PCR was set up as a simplex PCR detecting the target gene in one reaction and the housekeeping gene (RPL37A) for normalization in a second reaction. The final volume for the PCR reaction was 12.5 μl in a 1xPCR master mix, RPL37A primers were used in a final concentration of 50 nM and the probe of 200 nM. The ΔΔCt method was applied to calculate relative expression levels of the target transcripts. Percentage of target gene expression was calculated by normalization based on the levels of the LV3 non-silencing siRNA control sequence.

IC_{50} dose—response In-cell Western experiments were done in HepG2 cells using 10-step 5fold dilutions of Ambion's human CerS6 siRNA s48447 starting with 50 nM concentration. 15,000 HepG2 cells/well were reverse transfected in collagen-coated 96-well plates using 0.2 μl Lipofectamine RNAiMAX and incubation at 37 °C for 48 h. Cells were fixed with 3.7% formaldehyde for 20 min at room temperature followed by permeabilisation with 0.1% Triton X-100 for 4 × 5 min. Then wells were blocked by addition of 50 μl Odyssey Blocking Buffer (Li-COR#927-40000) and incubation at room temperature for 2 h. Incubation with primary CerS6 antibody (Abcam #ab56582) overnight at 4 °C was followed by treatment with secondary anti-mouse IRDye800CW antibody (Li-COR #926-32210) and CellTag 700 Stain (Li-COR #926-41090) for 1 h at room temperature. Plate readout was done using a Li-COR Odyssey CLx instrument.

Murine Hepa1-6 cells were reverse transfected with 10 nM CerS6 antisense oligonucleotides using 0.75 μl HiPerFect (Qiagen #301705) per 96-well according to the manufacturer's protocol and incubated at 37 °C for 48h. Isolated total RNA samples were assayed for CerS6 expression levels using the TaqMan Gene Expression assay Mm01270927_m1. Percentage of target gene expression was calculated by normalization based on the levels of the *C. elegans* anti-miR-67 control sequence.

Cell viability testing in Hepa1-6 cells was done using the CellTiter-Glo Assay (Promega #G7570) according to the supplier's protocol following a 10 nM ASO transfection and incubation for 72h. Percentage of cell viability was calculated by normalization based on the levels of the *C. elegans* anti-miR-67 control sequence.

 © 2019 The Authors. Published by Elsevier GmbH. This is an open access article under the CC BY-NC-ND license (http://creativecommons.org/licenses/by-nc-nd/4.0/).

2.2. Animal experiments

Knockdown efficacy of different ASO targeting CerS6 as well as dose response studies using CerS6 ASO (Figure 1) were conducted at Sanofi, Germany. For these experiments, healthy, male 8 week old C57BL/6J mice were obtained from Charles River (Germany). Mice were group-housed at room temperature in an environmentally controlled SPF-animal facility. Mice had ad libitum access to a standard rodent chow diet (Ssniff, Germany) as well as filtered tap water and were maintained on a 12 h light–dark cycle. Following acclimatization, mice were randomized into respective treatment groups. Mice received 3 injections of ASO (days 1, 4 and 8; s.c.) at the indicated doses (5 mL/kg) and were sacrificed 3 days after the third injection by cervical dislocation under isoflurane anesthesia for collection of plasma and tissues. All animal experimental procedures conducted at Sanofi were approved by the internal animal welfare committee as well as by German government authorities. All animal experiments which were carried out at Gubra were conducted in accordance with internationally accepted principles for the care and use of laboratory animals and were covered by a personal license issued for Jacob Jelsing (approved by the Danish Committee for Animal Research, permit number: 2013-15-2934-00784).

Male ob/ob and C57BL/6J HFD (DIO) obese and their respective lean control mice were used for the experiments carried out at Gubra. All animals were obtained from JanvierLabs, France. ob/ob and respective lean control mice were acclimatized for two-three weeks in their new environment with free access to standard rodent chow (#1324, Altromin, Lage, Germany). C57BL/6J DIO and lean control mice were fed D12492 60.0E%fat, Research Diets, New Brunswick, NJ, USA or standard rodent chow (#1324, Altromin, Lage, Germany), respectively, for 18 weeks, and domestic quality tap water. ob/ob

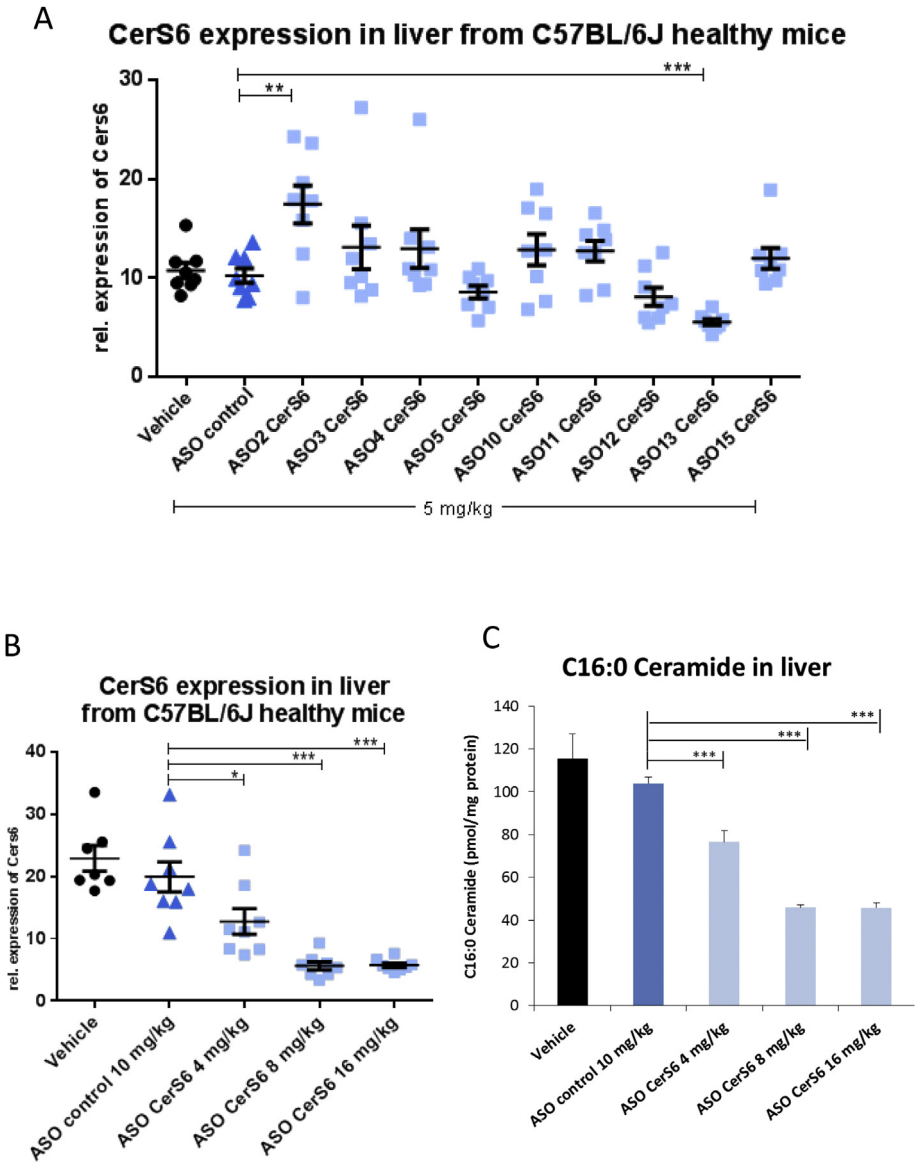

Figure 1: A: CerS6 mRNA expression levels in liver samples from C57BL/6J healthy mice treated with 5 mg/kg of nine different CerS6 ASO sequences, ASO control (*C. elegans* anti-miR-67) or PBS vehicle. Subcutaneous ASO injections were done at day 1 and 3, animals were sacrificed at day 5 (+/-SD). B: CerS6 mRNA expression levels in liver samples from C57BL/6J healthy mice treated with 4, 8 or 16 mg/kg of CerS6 ASO, 10 mg/kg ASO control (*C. elegans* anti-miR-67) or PBS vehicle. Subcutaneous ASO injections were done at day 1, 4 and 8, animals were sacrificed at day 11 (+/-SD). C: Liver C16:0 ceramide profiling from the same samples as shown in Figure 1B (+/-SEM).

 © 2019 The Authors. Published by Elsevier GmbH. This is an open access article under the CC BY-NC-ND license (http://creativecommons.org/licenses/by-nc-nd/4.0/).

and respective lean control mice were housed in groups of n = 5; C57BL/6J and lean control mice were single-housed. Body weight was recorded in connection with the dosing twice weekly from day −3 to day 45. Food and water intake was recorded daily from day −3 to 7; then weekly. During day 0−45 of the experiment, animals received twice weekly a subcutaneous dosing of either vehicle (PBS), the ASO control (10 mg/kg) or CerS6 ASO (10 mg/kg, dose reduced to 7.5 mg/kg after 3.5 weeks of treatment). ASO control and CerS6 ASO were dissolved in PBS at pH 7.4. On a non-dosing day, weekly intermittent blood samples were collected via tail vein for analysis of fed blood glucose, plasma insulin and the liver transaminsases ALT and AST.

2.3. Intra-peritoneal insulin tolerance test (ipITT)

Animals were fasted for 6 h prior to administration of the insulin bolus. Cages were changed at the time of fasting. Vehicle and test compounds were administered 1 h prior to the insulin bolus. At t = 0, mice received a bolus of human insulin (ob/ob mice received an insulin bolus of 1.5U/kg; lean control mice received an insulin bolus of 0.5U/kg. DIO mice received an insulin bolus of 1U/kg; lean chow fed control mice received an insulin bolus of 0.75U/kg (Humulin® R-U100; Eli Lilly)) by intra-peritoneal (i.p.) injection (5 ml/kg). Blood samples were collected from the tail vein and blood glucose was measured at time points −60, 0, 15, 30, 60 and 120 min after the insulin bolus. Mice were re-fed after the last blood sampling.

2.4. Oral glucose tolerance test (oGTT)

Animals were fasted for 6 h prior to administration of the glucose bolus. Cages were changed at the time of fasting. Vehicle and test compounds were administered 1 h prior to the glucose bolus. At t = 0, mice received an oral glucose load of 2 g/kg. Blood samples were collected from the tail vein and blood glucose was measured at time points −60, 0, 15, 30, 60, 120 and 180 min after the glucose administration. Samples for measuring HbA1c and plasma insulin collected in parallel at t = −60 and 15min, respectively. Mice were re-fed after the last blood sampling.

2.5. Whole body composition

Body composition analyzed prior to study start and before termination by non-invasive EchoMRI-900 (EchoMRI, USA). The scanner measured fat and lean tissue mass. During the scanning procedure, mice were placed in a restrainer for 90−120 s.

2.6. In-vivo pharmacology study termination

The day before termination (study day 44), whole body composition was determined using EchoMRI (prior to dosing). Animals were terminated on day 45 (last dose administered in the morning of day 43). Animals were fasted for 4 h prior to termination. Before sacrifice (at 10AM), blood samples were collected from the tail vein for measurement of blood glucose and plasma insulin. Thereafter (10AM−2PM), animals were terminated in a randomized order to take into account the time span between termination of the first and last animal.

2.7. Lipidomic profiling

HepG2 cells were detached from 96-well plates using 50% Detachin (Genlantis) and ceramides were extracted using 100% methanol. Ceramide species were determined using the RapidFire system with 6460 Triple-Quad SPE/MS (Agilent) and the RapidFire integrator program for data analyses. Mouse plasma or tissue homogenates were treated with 85% methanol/10% acetonitrile/5% water for ceramide extraction. Quantification of ceramides was done using an UltiMate 3000 system with TSQ Quantum Ultra Triple-Quad LC-MS instrumentation (Thermo/Finnigan).

2.8. Blood sampling

During anesthesia (isoflurane), the abdominal cavity was opened and cardiac blood was obtained for collection of terminal plasma (EDTA-heparin). These plasma samples were used for terminal analysis of the below detailed parameters.

2.9. Biochemistry

Blood glucose: Blood samples (tail vein) were collected into 10 µl heparinized glass capillary tubes, immediately suspended in buffer (0.5 ml of glucose/lactate system solution (EKF-diagnostics, Germany) and analyzed for glucose on the test day using a BIOSEN c-Line glucose meter (EKF-diagnostics, Germany) according to the manufacturer's instructions.

Triglyceride, total cholesterol, HDL cholesterol, ALT, AST, creatinine: Terminal plasma samples were used for these analyses. Samples were placed on ice and stored at −80 °C until analysis. Analytes were measured in single determinations using the autoanalyzer Cobas C-111 with commercial kits (Roche Diagnostics, Germany) according to the manufacturer's instructions.

Free fatty acids: 150 µl of terminal was blood collected into EDTA tubes containing 1% NaF (Sodium fluoride) and plasma was separated subsequently. Samples were stored at −80 °C until analysis. Free fatty acids were measured in single determinations using the autoanalyzer Cobas C-111 with a commercial kit (Wako, USA) according to the manufacturer's instructions.

Adiponectin and C-peptide: Terminal plasma was stored at −80 °C until analysis. Plasma samples were analyzed according to the manufacturer's instructions using the AlphaLisa kit (Perkin Elmer).

HbA1c: Blood samples were collected into 10 µl heparinized glass capillary tubes and immediately suspended in 1 ml haemolysate buffer (Roche Diagnostics, Germany). Samples were stored at −80 °C until analysis. HbA1C was measured in single determinations using autoanalyzer Cobas C-111 with commercial kit (Roche Diagnostics, Germany) according to the manufacturer's instructions.

Insulin: 50 µl blood was collected into heparinized tubes. Plasma was separated and samples stored at −80 °Celsius until analysis. Plasma was analysed using an AlphaLisa kit (Perkin Elmer), according to the manufacturer's instructions.

2.10. In-vivo CerS expression analysis

20−50 mg of frozen mouse tissue was used to extract total RNA using Qiagen's QIAzol and RNeasy reagents (#79306 and 74106). Expression levels of mouse CerS1, CerS2, CerS4, CerS5 and CerS6 were determined by applying the TaqMan Gene Expression assays Mm03024093_m1, Mm01258345_g1, Mm00482658_m1, Mm00510992_m1 and Mm01270927_m1, respectively.

3. RESULTS

Primarily we validated genetic knockdown of CerS6 in-vitro, using commercially available, pre-designed siRNAs in HepG2 cells. We evaluated three siRNA molecules from different manufactures to KD CerS6 mRNA. As shown in the supplementary information (Supplementary Table 1), two of the selected siRNAs (Ambion s48447 and s48448) reduced the CerS6 mRNA expression in a dose dependent manner by more than 90%. Furthermore, these siRNAs KD were highly selective against other CerS isoforms and did not affect expression of CerS2 or CerS5. Subsequently, we also confirmed the efficient and

 © 2019 The Authors. Published by Elsevier GmbH. This is an open access article under the CC BY-NC-ND license (http://creativecommons.org/licenses/by-nc-nd/4.0/).

dose dependent KD of CerS6 at the protein level by performing In-cell Western analyses (Supplementary Figure 1). Cellular CerS6 KD in HepG2 hepatocytes was associated with a significant and selective decrease in cellular C16:0 ceramide (Supplementary Figure 2a/b). These observations provided us proof-of-concept to specific ablation of CerS6 and corresponding selective decrease in the C16:0-ceramide production in-vitro. Next, this enabled us to pursue a nucleic acid based therapeutic approach to inhibit CerS6 in-vivo. In order to evaluate the effect of CerS6 inhibition also in extra-hepatic tissues, we favored antisense oligonucleotide (ASO) over siRNA technology as therapeutic modality. Subsequently, 15 CerS6 ASO molecules for in-vivo studies were designed and synthesized (Table 1). Initially, ASO molecules were tested for in-vitro KD potency and cytotoxicity in murine Hepa1-6 cells. Nine ASOs with >85% inhibition of CerS6 mRNA and >30% cellular viability at 10 nM concentration were selected (Supplementary Figure 3a&b). These nine ASO sequences were subsequently tested for in-vivo KD efficacy in healthy mice using two subcutaneous injections (5 mg/kg). As shown in Figure 1A, ASO #13 was found most active with a ~50% hepatic reduction of CerS6 mRNA expression. Eventually, ASO #13 (henceforth called as CerS6 ASO) was prioritized for further in-vivo pharmacological efficacy studies. Prior to longitudinal metabolic studies, we performed a dose titration target engagement analysis in healthy mice to select the optimal dose which achieved more than 70% liver CerS6 mRNA KD and leading to more than 50% hepatic C16:0 ceramide reduction (Figure 1B, C).

To investigate the metabolic effects of CerS6 inhibition in an appropriate rodent model, we initially profiled the liver and plasma C16:0 ceramide and liver CerS6 mRNA expression in three obese insulin-resistant or diabetic animal models (HFD obese, ob/ob and db/db mice) with respective lean controls. As shown in Figure 2A, ob/ob and HFD obese mice displayed significantly higher C16:0 ceramide levels as compared to lean mice (in the case of liver: female HFD obese mice only). No significant differences were observed in db/db vs. db/- mice. Based on these observations, we prioritized ob/ob mice as a suitable primary pharmacological rodent model to evaluation of CerS6 inhibition. In ob/ob mice, CerS6 expression was higher (Figure 2B) in the liver, brown adipose tissue (BAT), and subcutaneous white adipose tissue, respectively relative to lean control (not in epididymal adipose fat). The higher CerS6 expression in obese ob/ob mice was also correlated to a 4-fold increase of C16:0 ceramide in plasma and 2-fold increase in liver. As described in section one, previous CerS6 knockout studies conducted in HFD obese mice for thorough metabolic characterization, clearly displayed improved insulin sensitivity, higher whole body energy expenditure and improved glucose homeostasis [14]. In the current study, we aimed pharmacologically to investigate effect of CerS6 inhibition primarily in obese insulin resistance mice in an intervention setting using ASO as therapeutic modality.

First, we explored the effects of 6 weeks of longitudinal treatment with 10 mg/kg CerS6 ASO (S.C. twice weekly) in adult, male ob/ob mice. We determined the C16:0 ceramide levels in plasma/tissues and its association in pathophysiological conditions of obesity and insulin-resistance. The treatment with CerS6 ASO resulted in a significant knockdown of CerS6 in liver and restored the expression level observed in lean control animals (Figure 3A). Similarly, treatment with CerS6 ASO resulted in a significant knockdown of CerS6 in subcutaneous and epididymal white fat tissue (Supplementary Figure 4A&B). However, we did not see a CerS6 ASO mediated knockdown of CerS6 in brown adipose tissue (Supplementary Figure 4C). The CerS6 expression reduction in liver and white adipose tissue correlated well with the reduced C16:0 ceramide concentrations in liver and plasma (Figure 3B&C). Ceramide profiling, we had to restrict our analyses to liver and plasma due to limited availability of tissues and resources. However, previous studies which were performed in global and tissue specific CerS6 KO studies have investigated the full ceramide profile from several metabolic tissues [14]. Next, we have profiled the expression of the other CerS isoforms in major metabolic tissues for the selectivity of CerS6 ASO. As shown in the Supplementary Figures 5–7, CerS6 ASO did not affect the expression of the other CerS isoforms in metabolic tissues.

Major pharmacological readout parameters included body weight, body composition, insulin sensitivity and glucose homeostasis. Figure 4A shows the study outline for this experiment. After animal delivery, mice were fed with a standard chow diet and body weight, whole body fat mass and fed blood glucose (BG) were determined. Out of 40 delivered ob/ob mice, 30 mice were selected and randomized

Table 1 — List of CerS6 antisense oligonucleotides used for in-vitro and in-vivo experiments.

ASO ID	ASO length	Position in human CerS6 (NM_203463.2)	Position in mouse CerS6 (NM_172856.4)	ASO sequence[a] (5'–> 3')
CerS6 #01	16	1785–1800	–	AACGAGACTCTTGCAC
CerS6 #02	16	729–744	724–739	AATAGTAGTGAAGGTC
CerS6 #03	16	978–993	973–988	CAAACAGGAGATCACA
CerS6 #04	16	726–741	722–736	AGTAGTGAAGGTCAGT
CerS6 #05	15	979–993	974–988	CAAACAGGAGATCAC
CerS6 #06	16	976–991	971–986	AACAGGAGATCACACA
CerS6 #07	16	992–1007	–	CACGGCAAACATAACA
CerS6 #08	16	758–773	–	AGACCAATAAAACGAC
CerS6 #09	16	974–989	969–984	CAGGAGATCACACATT
CerS6 #10	15	816–830	811–825	CAGGAACATAATGCC
CerS6 #11	16	818–833	813–828	GTGCAGGAACATAATG
CerS6 #12	16	1145–1160	1140–1155	GTAAGACCAGAAGCAG
CerS6 #13	15	350–364	345–359	AAGATGAGCCGCACC
CerS6 #14	14	1011–1024	1006–1019	CGTGTGGTGATAAA
CerS6 #15	16	1033–1048	1028–1043	ACCCAGAGAGGAAATA
C. elegans anti-miR-67 (ASO Control)	16	–	–	*TCCTAGAAAGAGTAGA*[b]

[a] LNA spiking pattern in CerS6 ASO sequences proprietary to Exiqon. All sequences are fully phosphorothioated.
[b] Italic nucleotides = LNA, non-Italic nucleotides = DNA.

 © 2019 The Authors. Published by Elsevier GmbH. This is an open access article under the CC BY-NC-ND license (http://creativecommons.org/licenses/by-nc-nd/4.0/).

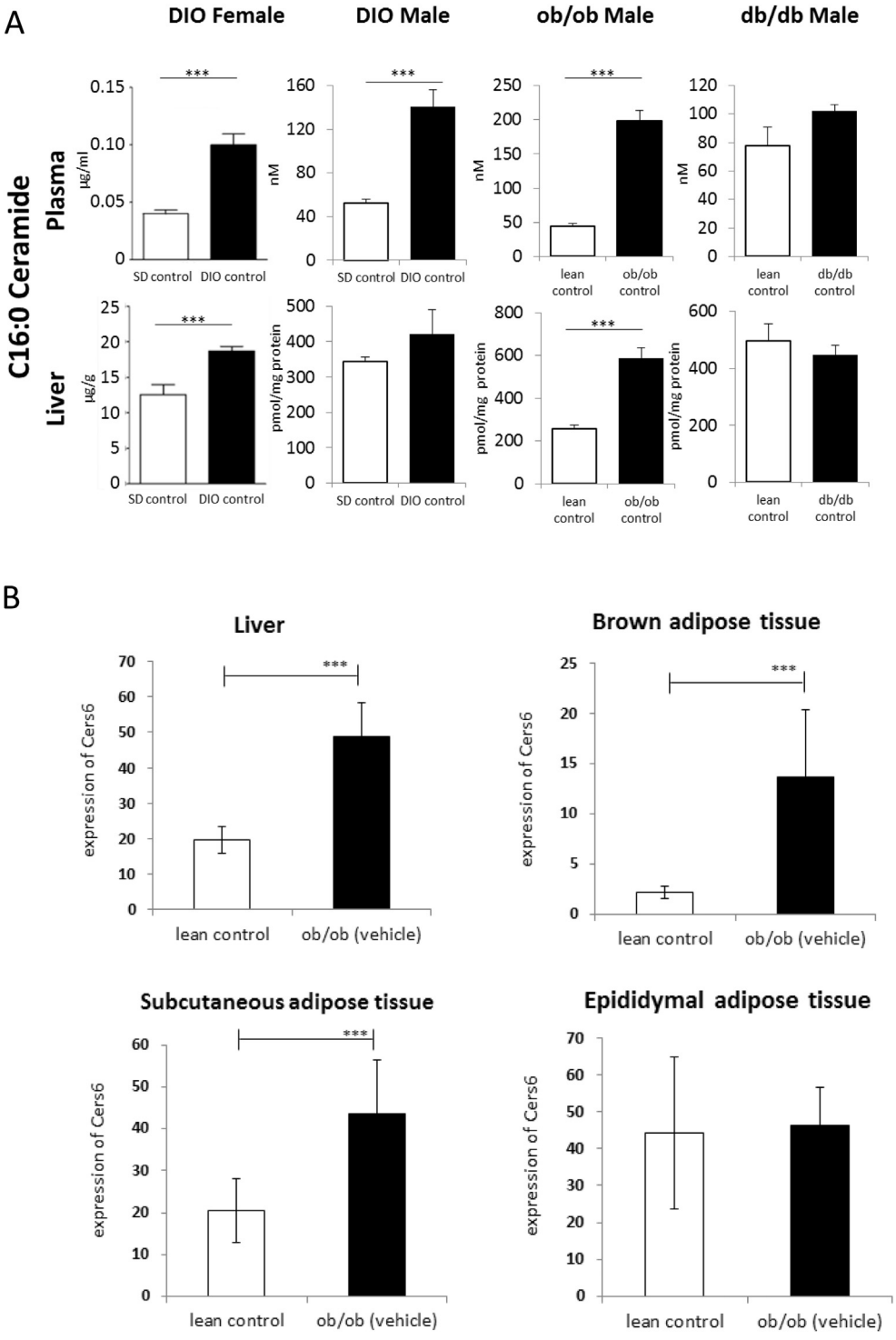

Figure 2: A: Liver and plasma C16:0 ceramide profiling from three obese and insulin-resistant/diabetic mouse models (male/female DIO, ob/ob and db/db) (+/-SEM). The statistical comparison between two groups was done with student's t tests. B: CerS6 mRNA expression levels in lean versus ob/ob mice in liver, brown adipose tissue, white subcutaneous and white epididymal adipose tissue and ileum (+/-SD). The statistical comparison between two groups was done with student's t-tests.

into the respective three treatment groups (n = 10/group). Selection/randomization of mice was carried out based on BW/whole body fat/BG measurements on day -3. The remaining animals were excluded from the main study. A 4th group (n = 10) of age matched lean mice served as an additional control group (ob/ob control). During the study period of 47 days, CerS6 ASO treatment did not affect the body weight change until day 35 as compared to ob/ob vehicle treated mice. However, a significant difference in body weight was observed at the end of the study (Figure 4B) with CerS6 ASO treatment. Notably, CerS6 ASO treatment significantly reduced morning fed blood glucose as compared to ob/ob vehicle and ASO control treated mice. After 35 days of treatment, fed BG in mice treated with ASO was even lower than in

 © 2019 The Authors. Published by Elsevier GmbH. This is an open access article under the CC BY-NC-ND license (http://creativecommons.org/licenses/by-nc-nd/4.0/).

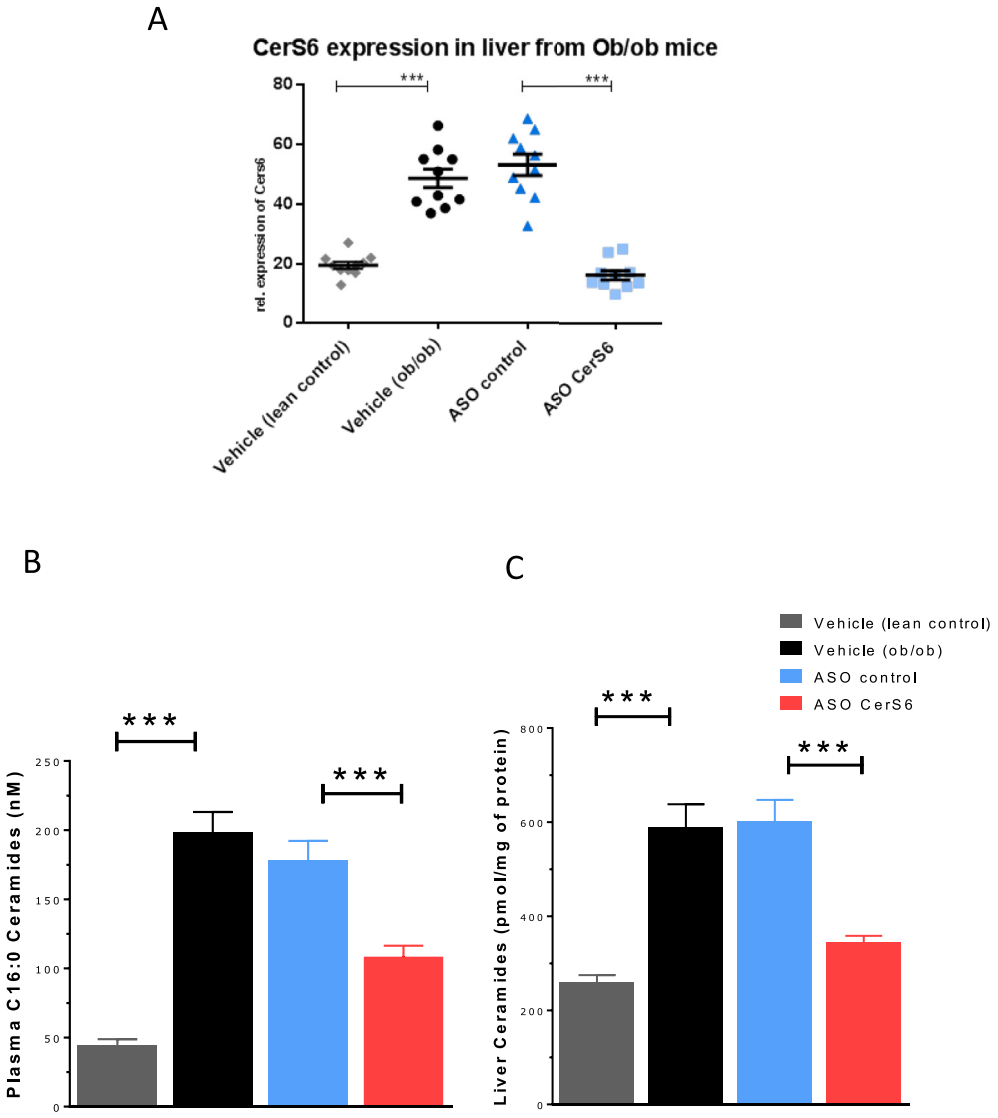

Figure 3: A: Terminal liver CerS6 mRNA expression profiling comparison between two groups statistical comparison done with student's t tests (+/-SEM). B&C: Terminal plasma and liver C16:0 ceramide profiling comparison between two groups statistical comparison was done with student's t tests (+/-SEM).

lean controls (Figure 4C). This significant glycemic control effect of CerS6 inhibition was further evidenced by a significant reduction of HbA1c levels with CerS6 ASO treatment at the end of the study (Figure 4D). Food intake was slightly reduced with CerS6 ASO treatment and the reduction was seen after 6th dose (~day 24), maintaining the same low food intake level until end of the study (Figure 4E). Moreover, CerS6 ASO treatment played a key role in the control of hyperinsulinemia in this obese and insulin resistant animal model by reducing morning plasma insulin as compared to vehicle and ASO control treated ob/ob mice. The reduction was evident after the 4th dosing and remained lower throughout the study (Figure 5A). During intra-peritoneal insulin tolerance tests (ipITT), CerS6 ASO treatment led to a significant improvement in glucose excursion after insulin treatment indicating a strong insulin sensitizing effect when compared to ob/ob vehicle and ASO controls (Figure 5B). Furthermore, CerS6 ASO treatment enhanced glucose clearance during oral glucose tolerance test (oGTT) as compared to ob/ob vehicle and ASO control (Figure 5C). CerS6 ASO treatment resulted in fasting blood glucose levels which were comparable to lean control mice (t = −60 min). Furthermore, CerS6 ASO displayed high peak blood glucose levels identical to ob/ob vehicle (t = 15 and 30 min post glucose bolus). However, the blood glucose rapidly reversed to baseline after 30 min post glucose bolus, resulting in a marked and significant reduction of AUC, comparable to the AUC observed in lean controls (Figure 5D). The calculation of the HOMA-IR from mice used in our experiments clearly shows that, compared with the lean control mice, ob/ob mice exhibited remarkable insulin resistance, as manifested by significant higher fasting serum insulin level (Figure 5E) and (HOMA-IR) index (Figure 5F). Treatment with CerS6 ASO significantly decreased fasting plasma insulin level and HOMA-IR in ob/ob mice (Figure 5E&F).

Next, we investigated in ob/ob mice how CerS6 ASO treatment affected body composition. Compared to vehicle treated ob/ob mice, multiple injections with CerS6 ASO significantly reduced body fat. Calculating the change in body fat measured before and after the treatment period, CerS6 ASO significantly decreased whole body fat at termination (0.5g). In contrast, in lean controls, ob/ob vehicle and ASO controls, whole body fat was increased at the end of the treatment period (Figure 6A). No significant changes in lean body mass, liver weight and

 © 2019 The Authors. Published by Elsevier GmbH. This is an open access article under the CC BY-NC-ND license (http://creativecommons.org/licenses/by-nc-nd/4.0/).

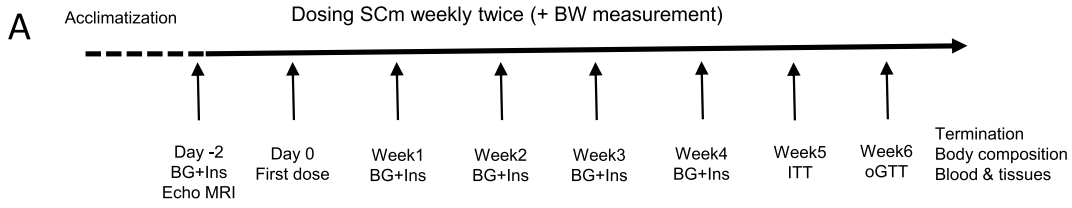

Male ob/ob mice 12 weeks of age prior to treatment

Group 1: Vehicle Lean control (PBS)

Group 2: ob/ob vehicle control (PBS)

Group 3: ob/ob ASO control 10 mg/kg

Group 4: ob/ob ASO CerS6 10 mg/kg, reduced to 7.5 mg/kg after 3.5 weeks

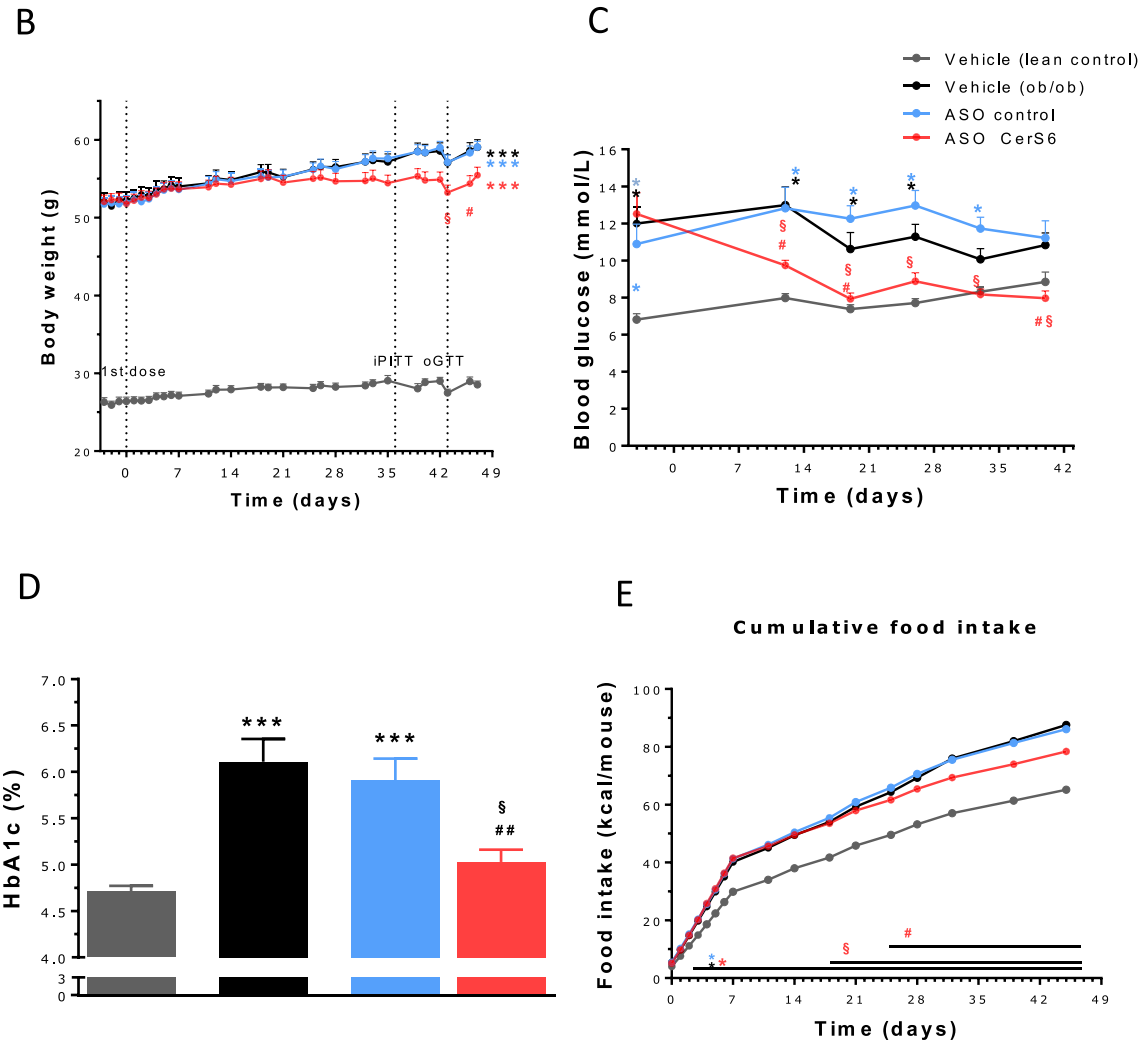

Figure 4: A: Graphical description of the study outline showing the longitudinal CerS6 ASO intervention efficacy study in ob/ob mice. B: Body weight (g) change during the study period of 47 days. The time of dosing start, ipITT, oGTT and dose change are marked with arrows. *p $<$ 0.05 as compared to lean control, #p $<$ 0.05 as compared to ob/ob vehicle, §p $<$ 0.05 as compared to ASO control (2-way ANOVA w/Bonferroni's post-hoc test). C&D: Weekly measurements of fed blood glucose and HbA1c measured prior to termination (day 43). Blood glucose samples were collected from the tail vein ~24 h post dosing. Blood glucose: *p $<$ 0.05 as compared to lean control, #p $<$ 0.05 as compared to ob/ob vehicle, §p $<$ 0.05 as compared to ASO control (2-way ANOVA w/Bonferroni's post-hoc test). HbA1c: ***p $<$ 0.001 as compared to lean control, ##p $<$ 0.01, ###p $<$ 0.001 as compared to ob/ob vehicle, §p $<$ 0.05, §§§p $<$ 0.001 as compared to ASO control (1-way ANOVA w/Bonferroni's post-hoc test). E: Daily and cumulative food intake measured up to day 45 during the study period of 47 days. *p $<$ 0.05 as compared to lean control, #p $<$ 0.05 as compared to ob/ob vehicle, §p $<$ 0.05 as compared to ASO control (2-way ANOVA w/Bonferroni's post-hoc test).

 © 2019 The Authors. Published by Elsevier GmbH. This is an open access article under the CC BY-NC-ND license (http://creativecommons.org/licenses/by-nc-nd/4.0/).

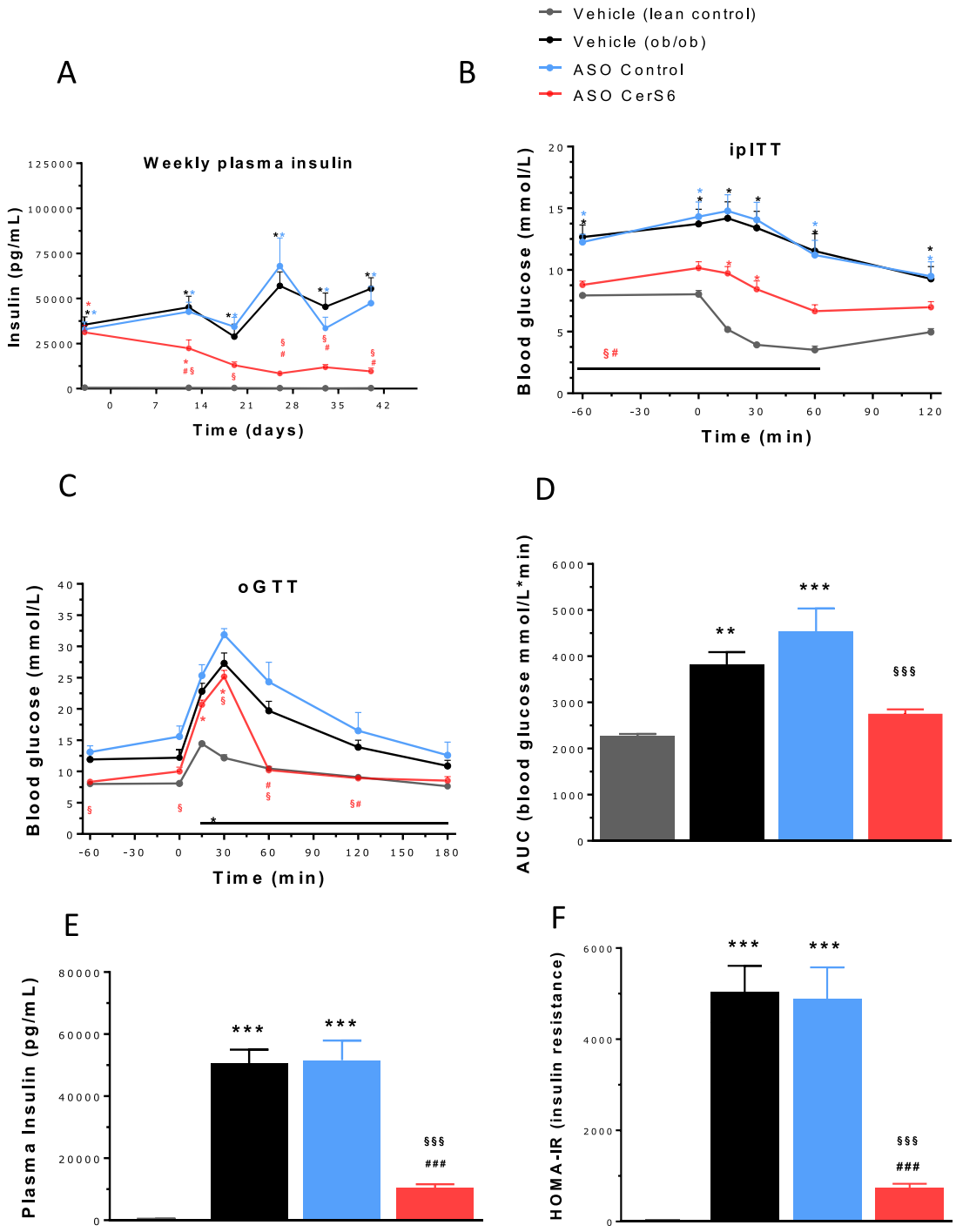

Figure 5: A: Weekly measurements of non-fasted plasma insulin. Samples were collected from the tail vein ~24 h post dosing. *p < 0.05 as compared to lean control, #p < 0.05 as compared to ob/ob vehicle, §p < 0.05 as compared to ASO control (2-way ANOVA w/Bonferroni's post-hoc test). B: Intraperitoneal insulin tolerance test (ipITT, time profile). The test was performed on study day 36, ~24 h post compound dosing at day 35. At t = 0, mice received a human insulin bolus (Humulin® R-U100; Eli Lilly) by i.p. injection (5 ml/kg). ob/ob mice received an insulin bolus of 1.5U/kg; lean control mice received an insulin bolus of 0.5U/kg. Time profile: *p < 0.05 as compared to lean control, #p < 0.05 as compared to ob/ob vehicle, §p < 0.05 as compared to ASO control (2-way ANOVA w/Bonferroni's post-hoc test). C: Oral glucose tolerance test (oGTT, time profile). The test was performed on study day 43, ~24 h post compound dosing at day 42. At t = 0, mice received a bolus of glucose (2 g/kg; 200 mg/ml) by oral gavage (10 ml/kg). Time profile: *p < 0.05 as compared to lean control, #p < 0.05 as compared to ob/ob vehicle, §p < 0.05 as compared to ASO control (2-way ANOVA w/Bonferroni's post-hoc test). D: AUC of oGTT: **p < 0.01, ***p < 0.001 as compared to lean control, ###p < 0.001 as compared to ob/ob vehicle, §§§p < 0.001 as compared to ASO control (1-way ANOVA w/Bonferroni's post-hoc test). E. terminal plasma insulin: *p < 0.05, ***p < 0.001 as compared to lean ob/- control; ##p < 0.01, ###p < 0.001 as compared to ob/ob vehicle; §p < 0.05, §§§p < 0.001 as compared to ASO control (1-way ANOVA w/Bonferroni's post-hoc test). F. HOMA-IR: *p < 0.05, ***p < 0.001 as compared to lean ob/- control; ##p < 0.01, ###p < 0.001 as compared to ob/ob vehicle; §p < 0.05, §§§p < 0.001 as compared to ASO control (1-way ANOVA w/Bonferroni's post-hoc test).

 © 2019 The Authors. Published by Elsevier GmbH. This is an open access article under the CC BY-NC-ND license (http://creativecommons.org/licenses/by-nc-nd/4.0/).

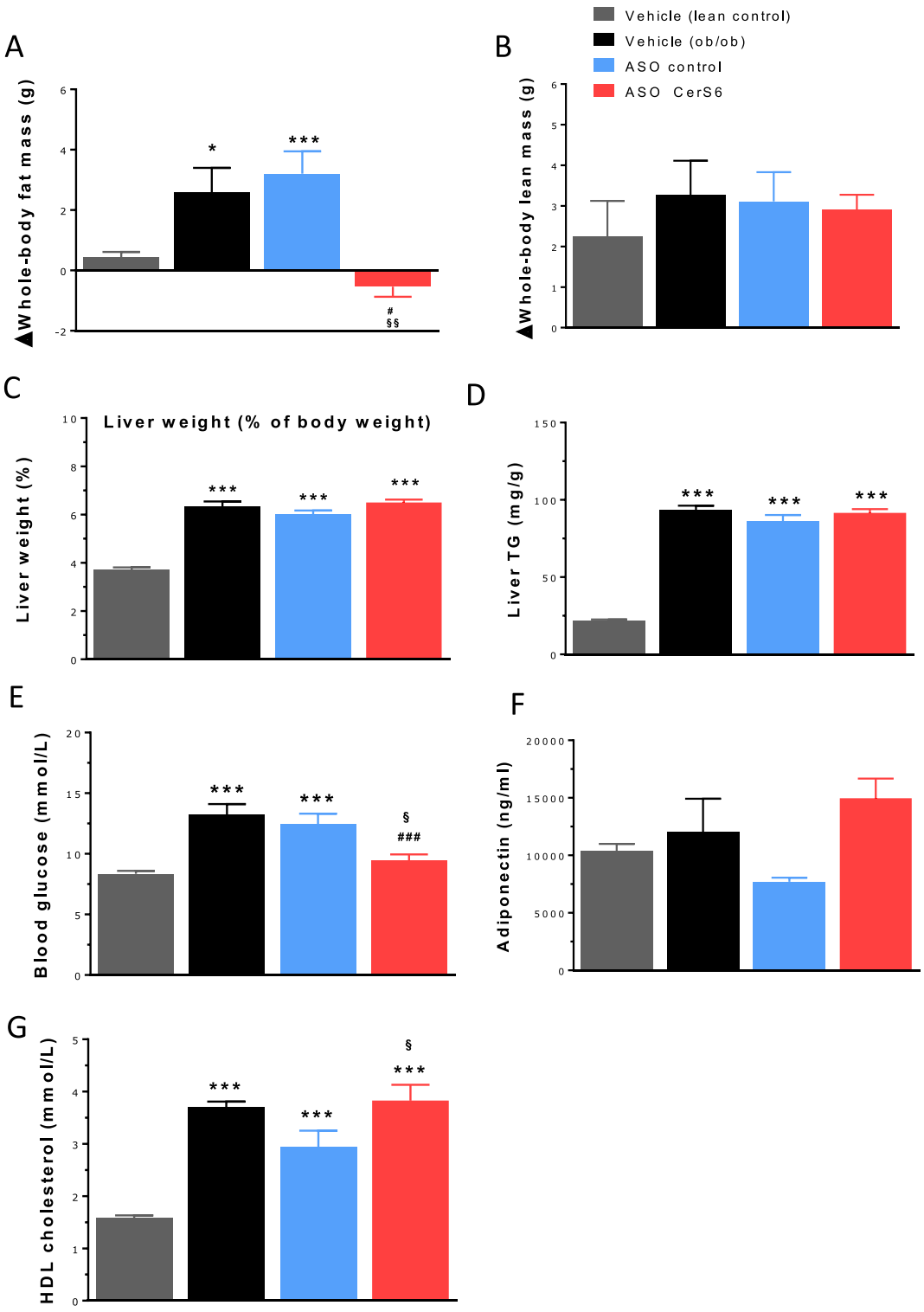

Figure 6: A: Whole body fat content (g) measured by EchoMRI scan at study day 46. *p < 0.05, ***p < 0.001 as compared to lean control, #p < 0.05, ##p < 0.01, ###p < 0.001 as compared to ob/ob vehicle, §§p < 0.01, §§§p < 0.001 as compared to ASO control (1-way ANOVA w/Bonferroni's post-hoc test). B: Whole body lean mass content (g) measured by EchoMRI scan at study day 46. C: Terminal liver weight – actual (g) and relative to body weight (%). ***p < 0.001 as compared to lean ob/- control, #p < 0.05, ###p < 0.001 as compared to ob/ob vehicle, p > 0.05 as compared to ASO control (1-way ANOVA w/Bonferroni's post-hoc test). D, E, F&G: Liver triglycerides, terminal blood glucose, terminal adiponectin and terminal HDL cholesterol, respectively *p < 0.05, ***p < 0.001 as compared to lean ob/- control; ##p < 0.01, ###p < 0.001 as compared to ob/ob vehicle; §p < 0.05, §§§p < 0.001 as compared to ASO control (1-way ANOVA w/Bonferroni's post-hoc test).

 © 2019 The Authors. Published by Elsevier GmbH. This is an open access article under the CC BY-NC-ND license (http://creativecommons.org/licenses/by-nc-nd/4.0/).

liver triglycerides were observed with treatment (Figure 6B, C&D). CerS6 ASO treatment significantly reduced terminal levels of blood glucose as compared to ob/ob vehicle (Figure 6E). Terminal plasma adiponectin concentrations were increased in the CerS6 ASO treatment group indicative for an insulin sensitizing effect of CerS6 inhibition (Figure 6F). In addition, we noticed a significant increase in plasma HDL-cholesterol concentrations in the CerS6 ASO treatment group. Thus, one may consider to further investigate potential cardio-protective effects of CerS6 inhibition (Figure 6G).

We also profiled the other species of ceramides in plasma and liver from the CerS6 ASO treated ob/ob and respective controls. As shown in Supplementary Figure 8b, very long chain ceramide levels were increased in CerS6 ASO treated ob/ob mice relative to ASO control treated mice. This was also associated with a significant increase in hepatic CerS2 expression. Higher CerS2 expression is likely responsible for the synthesis of very long chain ceramides in CerS6 ASO treated ob/ob relative to ASO control animals (Supplementary Figure 6D) and may be the consequence of improved insulin sensitivity. In this context, our previous [13] and recent findings [16] suggest a beneficial role of very long-chain sphingolipid species on glucose homeostasis and insulin action. Furthermore, a recent clinical study indicates that obesity and metabolic dysfunction are associated with short chain (C16:0) saturated fatty acid ceramide species and that a healthier metabolic profile was associated with longer-chain poly-unsaturated fatty acid ceramides [17]. We unfortunately not able to measure the sphingomyelin species of ceramides and consider this analysis to be out of scope for the current manuscript. Instead, we would like to highlight that Turpin et al. [14] already reported a comprehensive sphingomyelin profiling global and liver specific KO studies for CerS6.

Similarly, we have also explored the effects of a 6 weeks longitudinal treatment (S.C. twice weekly) with CerS6 ASO on body weight and body composition, insulin sensitivity and glucose homeostasis in adult, male HFD obese mice. Treatment with CerS6 ASO resulted in a significant knockdown of CerS6 were noticed in the liver (Supplementary Figure 9A). In line with the results obtained from the study in ob/ob mice, treatment with CerS6 ASO also resulted in a continuous body weight reduction reaching a terminal body weight, which was about 25% lower compared to vehicle treated HFD obese mice (Figure 7A). Important to note that, unlike in ob/ob, food intake was not affected by CerS6 ASO treatment in HFD obese mice and maintaining the similar level of food intake level until end of the study relative to vehicle control and ASO control HFD mice (Figure 7B). Again, lower body weight could quantitatively be explained by reduced fat mass while lean mass was not significantly different between CerS6 ASO and vehicle treated HFD obese mice (Figure 7C&D). In addition, unlike in ob/ob mice, we noticed a significant decrease in plasma triglyceride and liver triglyceride concentrations with CerS6 ASO treatment in DIO mice (Figure 7E&F).

Throughout the study, treatment with CerS6 ASO did not significantly affect fed blood glucose concentrations when compared to vehicle controls. However, fed plasma insulin concentrations were significantly lower with CerS6 ASO compared to vehicle treated HFD obese mice indicating that mice became more insulin sensitive (Figure 8A). The lack of treatment effects on blood glucose of HFD obese mice probably can be best explained by the only mild hyperglycemia in this cohort of mice, a feature that is frequently observed in this insulin resistance model mostly depending on the response of the individual mice to a high-fat diet [18] (fed blood glucose in HFD obese mice from the current study on study day "0" for lean mice: 8.5 mmol/L; for HFD-induced obese mice 9.0 mmol/L). Analysis of insulin sensitivity by insulin tolerance tests (ITT) after 5 weeks of treatment revealed a metabolically improved response to the insulin challenge with CerS6 ASO (Figure 8B). However, when calculating the corresponding AUC for the glucose curves, the respective group means failed to reach a statistically significant difference (data not shown). The calculation of the HOMA-IR from mice used in our experiments clearly shows that, compared with the lean control mice, HFD mice exhibited mild insulin resistance, as manifested by significant higher fasting serum insulin level (Figure 8C) and (HOMA-IR) index (Figure 8D). Treatment with CerS6 ASO decreased fasting plasma insulin level and HOMA-IR (Figure 8C,D) in HFD mice. After 6 weeks of treatment, HFD obese and lean mice were subjected to an oral glucose tolerance test, but treatment with CerS6 ASO did not significantly improve glucose excursion during oGTT (Figure 8E). However, CerS6 ASO treatment group displayed significantly lower insulin release vs. vehicle controls 15 min after the oral glucose bolus (Figure 8F). Moreover, terminal liver total glycogen concentrations and glycogen synthase gene expression increased in the CerS6 ASO treatment group of HFD obese mice relative to HFD ASO control mice an indicative for insulin sensitizing effect of CerS6 inhibition (Supplementary Figure 9B&C). In the line with ob/ob, terminal plasma adiponectin and HDL cholesterol concentrations were increased in the CerS6 ASO treatment group of HFD obese mice (Supplementary Figure 9D&E).

4. DISCUSSION AND CONCLUSION

Preclinical pharmacological and genetic studies demonstrated that inhibition of ceramide biosynthesis effectively reduces the accrual of total ceramides in most metabolic tissues which ameliorates liver steatosis, insulin resistance, type 2 diabetes, hypertension, and cardiomyopathy [8]. However, concerns exist about potential risks or adverse effects resulting from a global inhibition of sphingolipid biosynthesis for treatment of chronic diseases [13]. Therefore, for the first time, we demonstrated herein that therapeutic inhibition of a selective enzyme in the ceramide biosynthesis pathway being responsible for the formation of the deleterious C16:0 ceramide species can positively affect glucose metabolism. This approach led to a selective reduction of C16:0 ceramide whilst sparing other ceramide species unaffected. In this context, we characterized ob/ob and HFD obese mice to assess the CerS6 expression and C16:0 ceramide levels and found that CerS6 expression was significantly elevated in the liver and adipose tissues when compared to lean mice which is also correlated to elevated levels of plasma C16:0 ceramides. Consequently, we then considered the ob/ob and HFD obese mice models as highly suitable for the analysis of CerS6 inhibition. CerS6 ASO treatment efficiently reduced the CerS6 expression in liver, subcutaneous and visceral fat, but not in brown adipose tissue. The reduced tissue expression was paralleled by a significant, 50% reduction of C16:0 ceramides in plasma. These observations indicate that circulating plasma C16:0 ceramides are mostly generated from liver and white adipose tissue. ASO mediated CerS6 inhibition resulted in improved glucose tolerance and insulin sensitivity as well as in a significant reduction of fed blood glucose in ob/ob mice. Moreover, insulin sensitivity was significantly improved during ITT and glucose handling was enhanced during oGTT. Finally, a significant reduction of body weight was observed with CerS6 ASO treatments. Consistent with previous CerS6 knockout studies, HFD-fed obese mice treated with CerS6 ASO displayed a significant (25%) weight reduction that was not associated with a reduction in food intake. Unlike in HFD obese mice, differential effect of CerS6 ASO in ob/ob mice on mild reduced food intake possibly associated improved hypothalamic inflammation in

 © 2019 The Authors. Published by Elsevier GmbH. This is an open access article under the CC BY-NC-ND license (http://creativecommons.org/licenses/by-nc-nd/4.0/).

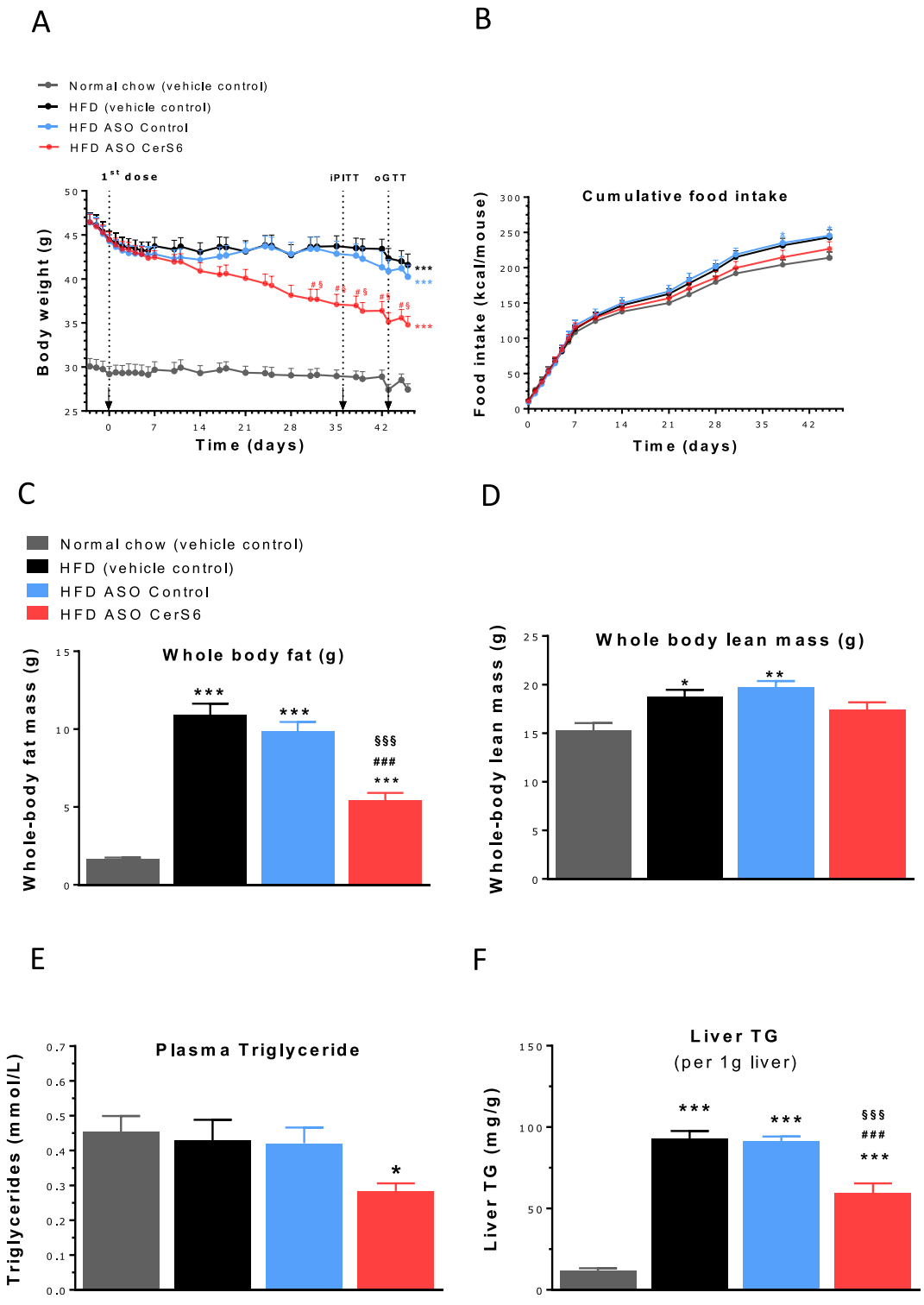

Figure 7: A: Body weight (g) change during the study period of 47 days. The time of dosing start, ipITT, oGTT and dose change are marked with arrows. ***p $<$ 0.001 as compared to normal chow lean control, #p $<$ 0.05 as compared to HFD vehicle control, §p $<$ 0.05 as compared to HFD ASO control (2-way ANOVA w/Bonferroni's post-hoc test). B: Daily and cumulative food intake measured up to day 45 during the study period of 47 days. *p $<$ 0.05 as compared to lean control, (2-way ANOVA w/Bonferroni's post-hoc test). C: Whole body fat content (g) measured by EchoMRI scan at study day 46. ***p $<$ 0.001 as compared to normal chow lean control, ###p $<$ 0.001 as compared to HFD vehicle control, §§§p $<$ 0.001 as compared to HFD ASO control (1-way ANOVA w/Bonferroni's post-hoc test). D: Whole body lean mass content (g) measured by EchoMRI scan at study day 46. *p $<$ 0.05, **p $<$ 0.01 as compared to normal chow lean control. E: Terminal plasma triglycerides. *p $<$ 0.05 as compared to normal chow lean control (1-way ANOVA w/Bonferroni's post-hoc test). F: Terminal liver triglycerides. ***p $<$ 0.001 as compared to normal chow lean control, #p $<$ 0.05, ###p $<$ 0.001 as compared to HFD vehicle control, §§§p $<$ 0.001 as compared to HFD ASO control (1-way ANOVA w/Bonferroni's post-hoc test).

 © 2019 The Authors. Published by Elsevier GmbH. This is an open access article under the CC BY-NC-ND license (http://creativecommons.org/licenses/by-nc-nd/4.0/).

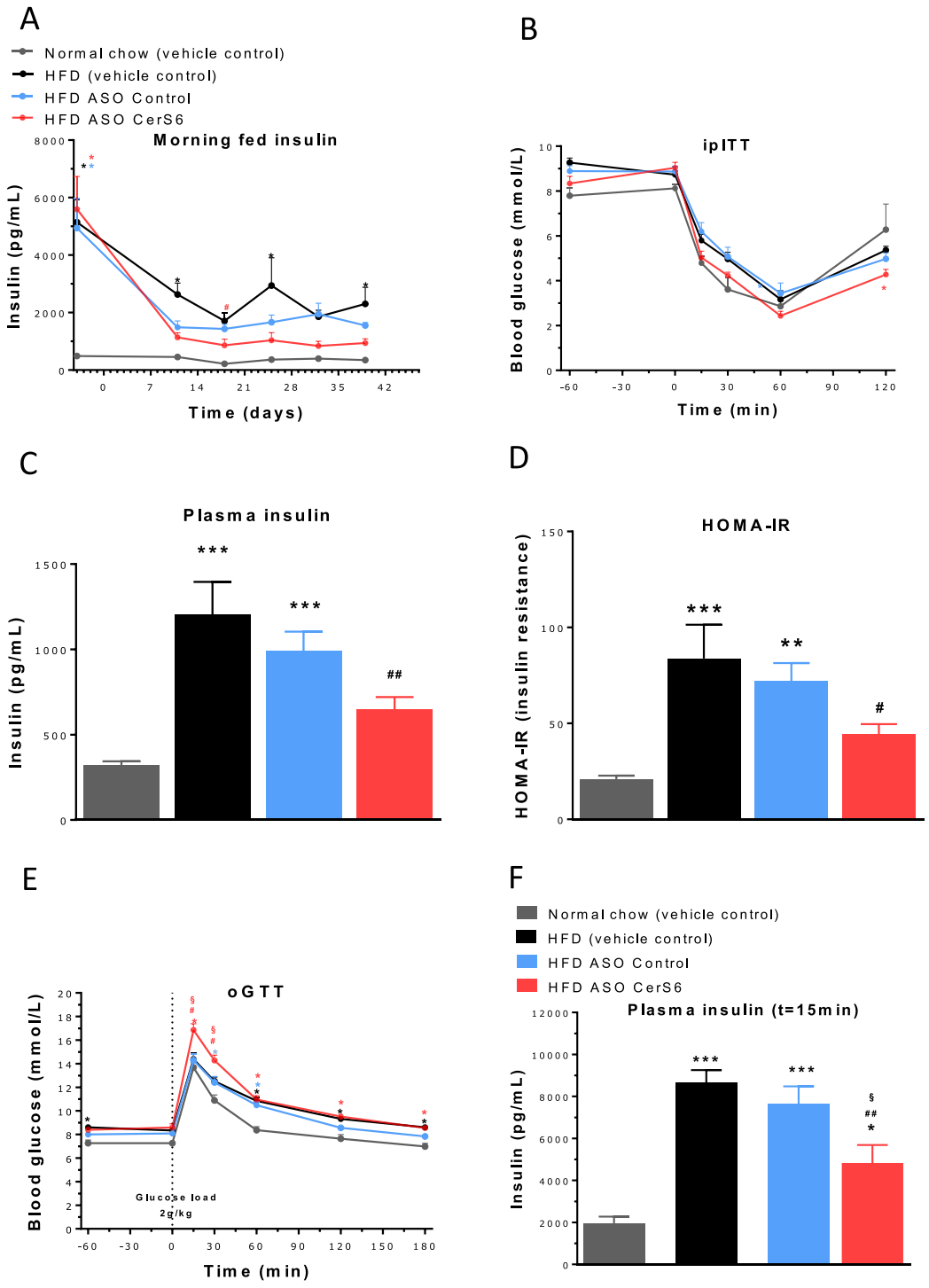

Figure 8: A: Weekly measurements of non-fasted plasma insulin. Samples were collected from the tail vein ~24 h post dosing. *p < 0.05 as compared to lean control, #p < 0.05 as compared to ob/ob vehicle, §p < 0.05 as compared to ASO control (2-way ANOVA w/Bonferroni's post-hoc test). B: Intraperitoneal insulin tolerance test (ipITT, time profile). The test was performed on study day 36, ~24 h post compound dosing at day 35. At t = 0, mice received a human insulin bolus (Humulin® R-U100; Eli Lilly) by i.p. injection (5 ml/kg). HFD mice received an insulin bolus of 1U/kg; normal chow lean control mice received an insulin bolus of 0.75U/kg. Time profile: *p < 0.05 as compared to lean control, #p < 0.05 as compared to HFD vehicle, §p < 0.05 as compared to HFD ASO control (2-way ANOVA w/Bonferroni's post-hoc test). D: terminal plasma insulin: *p < 0.05 and ***p < 0.001 as compared to normal chow lean control, ##p < 0.01 as compared to HFD vehicle, §p < 0.05 as compared to HFD ASO control (2-way ANOVA w/Bonferroni's post-hoc test). E: HOMA-IR: *p < 0.05 and ***p < 0.001 as compared to normal chow lean control, ##p < 0.01 as compared to HFD vehicle, §p < 0.05 as compared to HFD ASO control (2-way ANOVA w/Bonferroni's post-hoc test). F: Oral glucose tolerance test (oGTT, time profile). The test was performed on study day 43, ~24 h post compound dosing at day 42. At t = 0, mice received a bolus of glucose (2 g/kg; 200 mg/ml) by oral gavage (10 ml/kg). Time profile: *p < 0.05 as compared to lean control, #p < 0.05 as compared to ob/ob vehicle, §p < 0.05 as compared to ASO control (2-way ANOVA w/Bonferroni's post-hoc test). F: Plasma insulin measurement after 15 min glucose challenge during oral glucose tolerance test. *p < 0.05 and ***p < 0.001 as compared to normal chow lean control, ##p < 0.01 as compared to HFD vehicle, §p < 0.05 as compared to HFD ASO control (2-way ANOVA w/Bonferroni's post-hoc test).

 © 2019 The Authors. Published by Elsevier GmbH. This is an open access article under the CC BY-NC-ND license (http://creativecommons.org/licenses/by-nc-nd/4.0/).

CerS6 ASO treatment in leptin deficient ob/ob mice. Therefore, further investigations are warranted to elucidate the role of CerS6 in hypothalamic inflammation and leptin signaling [19]. Secondly, we noticed a significant reduction of liver and plasma triglycerides in CerS6 ASO HFD mice. However, CerS6 ASO treated ob/ob mice displayed unchanged liver/plasma triglycerides, possibly due to diminished leptin signaling in the liver. In this context, another study suggests that the lack of hepatic leptin signalling results in increased lipid accumulation in the liver specifically triglyceride-rich VLDL particles [20]. Moreover, previous studies demonstrated that weakened leptin signalling in db/db mice results in decreased liver ceramides possibly due to lipid membrane decomposition via an inflammatory response [21]. This is consistent with our observation that livers of db/db mice displayed reduced ceramide concentrations. Our therapeutic experiments in ob/ob and HFD obese mice confirmed the key metabolic benefits CerS6 inhibition such as insulin sensitization, improvement in hyperglycemia and more importantly reduced body weight. These findings are in contrast to PPARγ agonists which are currently the only insulin sensitizers used in the clinical setting. Moreover, their use is associated with an undesired side effects and increase in body weight. CerS6 inhibition also resulted in an elevation of circulating adiponectin levels and increased liver glycogen content possibly due to improved insulin sensitivity.

Several clinical studies demonstrated that elevated ceramides in plasma and metabolic tissues such as in skeletal muscle, liver and adipose tissue may have implications in the development of insulin resistance, obesity and major adverse cardiovascular events [15,22]. In this context, our present findings in insulin resistant and obese ob/ob mice display significant higher expression of CerS6 in liver and subcutaneous fat (not in epididymal fat) (Supplementary Figure 6). Secondly, we also profiled CerS6 expression in samples from human subjects. In visceral and subcutaneous fat of 10 non-diabetic obese and of 15 non-diabetic lean control subjects, we found that CerS6 expression was significantly elevated (1.4-fold) in subcutaneous fat (not in visceral fat) of obese relative to lean control subjects (Supplementary Figure 11). These observations are consistent with a recent report from Chaurasia et al. [23] who also showed a significant increase of C16:0 ceramides in subcutaneous fat (but not in visceral fat) of obese subjects with type 2 diabetes. Additionally, Turpin et al. investigated the role of CerS6 on insulin resistance in global KO and organ specific KO animals [14]. In these studies, demonstrated that the dysregulation of CerS6 promotes insulin resistance and obesity mainly through liver and brown adipose tissue (not through skeletal muscle). Independent of the target, increased circulating concentrations of liver transaminases, being indicative of hepatic damage, are commonly observed with LNA gapmer antisense oligonucleotide [24–27] therapeutics. In the current study, we have also measured plasma ALT and AST concentrations throughout the study and noted an increase in these enzymes after three weeks of treatment. Consequently, after 3 $^1/_2$ weeks of treatment, we reduced the dose to 7.5 mg/kg s.c. twice weekly. With the lower ASO dose, liver enzymes largely normalized towards the end of the study in both ob/ob and HFD obese animals (Supplementary Figure 10). We believe that this increase in liver enzymes was due to nonspecific effects of ASO and not connected to the CerS6 ablation. Furthermore, our previous studies in global and hepatic CerS6 knockout mice fed with control or high fat diets did not display any hepatic toxicity [13].

The studies herein suggest that CerS6 should specifically be targeted for the reduction of C16:0 ceramides, and by using the ASO technology we validated that CerS6 could be a novel target to reduce the accumulation of deleterious C16:0 ceramides in vivo. In conclusion, CerS6 mediated C16:0 ceramide reduction could be a potentially attractive target for the treatment of insulin resistance, obesity and type 2 diabetes.

AUTHOR CONTRIBUTIONS

S.R. (was an employee of Sanofi-Aventis during this project completion) wrote the manuscript and performed experiments in association with the contract research organization 'Gubra Aps' Denmark shown in Figures 3–8 and all Supplementary Figures. B.B. contributed to the experiments shown in Figures 1 and 2 and Supplementary Figures 1, 3–7, 9 & 11. M.B. designed, conducted and interpreted ASO-treatment studies in healthy mice and contributed to design and interpretation of in-vivo studies in ob/ob and DIO mice. B.W. contributed to the lipidomic analyses in Figure 2. A.P. contributed to the lipidomic analyses in Figures 1–3 and Supplementary Figure 8. G.H. conducted and coordinated all in-vivo experiments in ob/ob and DIO mice carried out at Gubra. N.T., J.C.B., and P.J.L. oversaw the project. All authors contributed to the final editing of the manuscript.

ACKNOWLEDGMENTS

This work was supported by Anja Kissel, Mike Helms, Jutta Rosenberger, Christiane Metz-Weidmann and Ralf Katzenmeier (Sanofi), Sarah Turpin-Nolan (Max Planck Institute for Metabolic Research), Jacob Jelsing and Niels Vrang (Gubra Aps) and Niels Frandsen (Exiqon). The authors declare no conflict of interests. Dr. Norbert Tennagels is the guarantor of this work and, as such, had full access to all the data in the study and takes responsibility for the integrity of the data and the accuracy of the data analysis.

CONFLICT OF INTEREST

S.R. is presently an employee of Evotec International GmbH, Germany. G.H. is an employee of Gubra ApS, Denmark. J.C.B. is an employee of Max Plank institute for metabolic research, Germany. B.B., M.B., A.P., B.W., and N.T. are employees of Sanofi-Aventis, Germany. PJL is an employee of Grünenthal, Germany.

APPENDIX A. SUPPLEMENTARY DATA

Supplementary data to this article can be found online at https://doi.org/10.1016/j.molmet.2018.12.008.

REFERENCES

[1] Mittermayer, F., Caveney, E., De Oliveira, C., Gourgiotis, L., Puri, M., Tai, L.J., et al., 2015. Addressing unmet medical needs in type 2 diabetes: a narrative review of drugs under development. Current Diabetes Reviews 11:17–31.

[2] Gao, Y., Bielohuby, M., Fleming, T., Grabner, G.F., Foppen, E., Bernhard, W., et al., 2017. Dietary sugars, not lipids, drive hypothalamic inflammation. Molecular Metabolism 6:897–908.

[3] Meikle, P.J., Summers, S.A., 2016. Sphingolipids and phospholipids in insulin resistance and related metabolic disorders. Nature Reviews Endocrinology.

[4] Yi, C.X., Walter, M., Gao, Y., Pitra, S., Legutko, B., Kalin, S., et al., 2017. TNFalpha drives mitochondrial stress in POMC neurons in obesity. Nature Communications 8:15143.

[5] Holland, W.L., Bikman, B.T., Wang, L.P., Yuguang, G., Sargent, K.M., Bulchand, S., et al., 2011. Lipid-induced insulin resistance mediated by the proinflammatory receptor TLR4 requires saturated fatty acid-induced ceramide biosynthesis in mice. Journal of Clinical Investigation 121:1858–1870.

[6] Hu, W., Ross, J., Geng, T., Brice, S.E., Cowart, L.A., 2011. Differential regulation of dihydroceramide desaturase by palmitate versus monounsaturated

 © 2019 The Authors. Published by Elsevier GmbH. This is an open access article under the CC BY-NC-ND license (http://creativecommons.org/licenses/by-nc-nd/4.0/).

fatty acids: implications for insulin resistance. Journal of Biological Chemistry 286:16596–16605.

[7] Bikman, B.T., Summers, S.A., 2011. Ceramides as modulators of cellular and whole-body metabolism. Journal of Clinical Investigation 121:4222–4230.

[8] Chavez, J.A., Summers, S.A., 2012. A ceramide-centric view of insulin resistance. Cell Metabolism 15:585–594.

[9] Chaurasia, B., Summers, S.A., 2015. Ceramides - lipotoxic inducers of metabolic disorders. Trends in Endocrinology and Metabolism 26:538–550.

[10] Stratford, S., Hoehn, K.L., Liu, F., Summers, S.A., 2004. Regulation of insulin action by ceramide: dual mechanisms linking ceramide accumulation to the inhibition of Akt/protein kinase B. Journal of Biological Chemistry 279:36608–36615.

[11] Hage Hassan, R., Pacheco de Sousa, A.C., Mahfouz, R., Hainault, I., Blachnio-Zabielska, A., Bourron, O., et al., 2016. Sustained action of ceramide on the insulin signaling pathway in muscle cells: implication of the double-stranded RNA-activated protein kinase. Journal of Biological Chemistry 291:3019–3029.

[12] Merrill Jr., A.H., 2011. Sphingolipid and glycosphingolipid metabolic pathways in the era of sphingolipidomics. Chemistry Review 111:6387–6422.

[13] Raichur, S., Wang, S.T., Chan, P.W., Li, Y., Ching, J., Chaurasia, B., et al., 2014. CerS2 haploinsufficiency inhibits beta-oxidation and confers susceptibility to diet-induced steatohepatitis and insulin resistance. Cell Metabolism 20:687–695.

[14] Turpin, S.M., Nicholls, H.T., Willmes, D.M., Mourier, A., Brodesser, S., Wunderlich, C.M., et al., 2014. Obesity-induced CerS6-dependent C16:0 ceramide production promotes weight gain and glucose intolerance. Cell Metabolism 20:678–686.

[15] Larsen, P.J., Tennagels, N., 2014. On ceramides, other sphingolipids and impaired glucose homeostasis. Molecular Metabolism 3:252–260.

[16] Montgomery, M.K., Brown, S.H., Lim, X.Y., Fiveash, C.E., Osborne, B., Bentley, N.L., et al., 2016. Regulation of glucose homeostasis and insulin action by ceramide acyl-chain length: a beneficial role for very long-chain sphingolipid species. Biochimica et Biophysica Acta 1861:1828–1839.

[17] Neeland, I.J., Singh, S., McGuire, D.K., Vega, G.L., Roddy, T., Reilly, D.F., et al., 2018. Relation of plasma ceramides to visceral adiposity, insulin resistance and the development of type 2 diabetes mellitus: the Dallas Heart Study. Diabetologia 61:2570–2579.

[18] Peyot, M.L., Pepin, E., Lamontagne, J., Latour, M.G., Zarrouki, B., Lussier, R., et al., 2010. Beta-cell failure in diet-induced obese mice stratified according to body weight gain: secretory dysfunction and altered islet lipid metabolism without steatosis or reduced beta-cell mass. Diabetes 59:2178–2187.

[19] Jais, A., Bruning, J.C., 2017. Hypothalamic inflammation in obesity and metabolic disease. Journal of Clinical Investigation 127:24–32.

[20] Huynh, F.K., Neumann, U.H., Wang, Y., Rodrigues, B., Kieffer, T.J., Covey, S.D., 2013. A role for hepatic leptin signaling in lipid metabolism via altered very low density lipoprotein composition and liver lipase activity in mice. Hepatology 57:543–554.

[21] Kim, K.E., Jung, Y., Min, S., Nam, M., Heo, R.W., Jeon, B.T., et al., 2016. Caloric restriction of db/db mice reverts hepatic steatosis and body weight with divergent hepatic metabolism. Scientific Reports 6:30111.

[22] Meeusen, J.W., Donato, L.J., Bryant, S.C., Baudhuin, L.M., Berger, P.B., Jaffe, A.S., 2018. Plasma ceramides: a novel predictor of major adverse cardiovascular events after coronary angiography. Arteriosclerosis, Thrombosis, and Vascular Biology.

[23] Chaurasia, B., Kaddai, V.A., Lancaster, G.I., Henstridge, D.C., Sriram, S., Galam, D.L., et al., 2016. Adipocyte ceramides regulate subcutaneous adipose browning, inflammation, and metabolism. Cell Metabolism 24:820–834.

[24] Burdick, A.D., Sciabola, S., Mantena, S.R., Hollingshead, B.D., Stanton, R., Warneke, J.A., et al., 2014. Sequence motifs associated with hepatotoxicity of locked nucleic acid–modified antisense oligonucleotides. Nucleic Acids Research 42:4882–4891.

[25] Burel, S.A., Hart, C.E., Cauntay, P., Hsiao, J., Machemer, T., Katz, M., et al., 2016. Hepatotoxicity of high affinity gapmer antisense oligonucleotides is mediated by RNase H1 dependent promiscuous reduction of very long pre-mRNA transcripts. Nucleic Acids Research 44:2093–2109.

[26] Hagedorn, P.H., Yakimov, V., Ottosen, S., Kammler, S., Nielsen, N.F., Hog, A.M., et al., 2013. Hepatotoxic potential of therapeutic oligonucleotides can be predicted from their sequence and modification pattern. Nucleic Acid Therapeutics 23:302–310.

[27] Stanton, R., Sciabola, S., Salatto, C., Weng, Y., Moshinsky, D., Little, J., et al., 2012. Chemical modification study of antisense gapmers. Nucleic Acid Therapeutics 22:344–359.

 © 2019 The Authors. Published by Elsevier GmbH. This is an open access article under the CC BY-NC-ND license (http://creativecommons.org/licenses/by-nc-nd/4.0/).